

Local-density-functional calculations of the vacancy-oxygen center in Ge

A. Carvalho* and R. Jones

School of Physics, University of Exeter, Stocker Road, Exeter EX4 4QL, United Kingdom

J. Coutinho and V. J. B. Torres

Department of Physics, University of Aveiro, 3810 Aveiro, Portugal

S. Öberg

Department of Mathematics, Luleå University of Technology, Luleå S-97187, Sweden

J. M. Campanera Alsina

CPES, University of Sussex, Falmer, Brighton BN1 9QJ, United Kingdom

M. Shaw and P. R. Briddon

School of Natural Sciences, University of Newcastle upon Tyne, Newcastle upon Tyne NE1 7RU, United Kingdom

(Received 8 August 2006; revised manuscript received 20 October 2006; published 30 March 2007)

We carry out a comprehensive density-functional study of the vacancy-oxygen (VO) center in germanium using large H-terminated Ge clusters. The importance of a nonlinear core correction to account for the involvement of the 3d electrons in Ge-O bonds is discussed. We calculate the electrical levels and the vibrational modes of VO^0 , VO^- , and VO^- finding close agreement with experiment. We also explore the reorientation, migration, and dissociation mechanisms of neutral and negatively charged VO and compare the calculated energy barriers with experimental data. We conclude that the defect is likely to anneal through both mechanisms.

DOI: [10.1103/PhysRevB.75.115206](https://doi.org/10.1103/PhysRevB.75.115206)

PACS number(s): 61.72.Bb, 61.72.Ji, 68.55.Ln, 71.55.Cn

I. INTRODUCTION

The vacancy-oxygen (VO) complex, or A center, is one of the dominant defects in oxygen-rich irradiated silicon and germanium, and is formed around 60 K when a mobile lattice vacancy (V) produced by irradiation is trapped by an interstitial oxygen atom (O_i).

The earliest reports on the VO center in Ge date back to electron paramagnetic resonance (EPR) measurements by Baldwin¹ and infrared (IR) measurements by Whan.² The identification of the defect was mainly based on the analogy of its properties with those of the corresponding defect in silicon. Despite the difficulties with the EPR measurements in ^{nat}Ge, Baldwin¹ deduced a structure for VO^- analogous with the model of Watkins and Corbett for the A center in Si.³ The C_{2v} symmetry has been confirmed in a recent study performed on ⁷⁴Ge enriched samples.⁴ In analogy with Si, the VO center in Ge was therefore expected to possess an acceptor level, and this has been supported by deep level transient spectroscopy (DLTS) and electrical measurements.⁵⁻⁹ However, surprisingly, Markevich *et al.*,¹⁰ using DLTS and Fourier transform infrared (FTIR) spectroscopy, found that in contrast with Si, the A center in Ge has, not two, but three charge states: neutral (VO^0), single negative (VO^-), and double negative (VO^{2-}). The same work reported ($-/0$) and ($=/-$) electrical levels at $E_v+0.27$ eV and $E_c-0.21$ eV, respectively.¹⁰ Three IR absorption bands at 621, 669, and 716 cm^{-1} were assigned to the asymmetric stretch mode of the Ge-O-Ge unit in VO^0 , VO^- , and VO^{2-} , respectively.^{4,11}

Previous local-density-functional calculations carried out in 64 atom supercells accurately placed the frequency of the local vibrational mode (LVM) of the neutral defect at

642 cm^{-1} ,¹² but in contrast with calculations in Si, found neutral and single negatively charged defects to have identical structures and very close local vibrational modes. However, the evidence supporting the assignment of the 669 cm^{-1} (in ¹⁶O-rich Ge) and 635 cm^{-1} (in ¹⁸O-rich Ge) bands to the asymmetric stretch of VO^- is very strong. The fine structures of these bands arising from different Ge isotopic combinations were accurately fitted by a quasimolecular Ge-O-Ge model.⁴ Moreover, the identical annealing behavior of the FTIR and DLTS signals strongly supports the assignment of all three vibrational bands at 621, 669, and 716 cm^{-1} and both acceptor levels to the same defect.^{4,10,11,13} The difficulties in modeling the negative charge state have been attributed to the very small or negative energy gap (-0.06 eV in Ref. 14) found in density-functional calculations for Ge. Thus, an electron added to the supercell enters the conduction band and is not localized on the defect. In contrast, a cluster calculation leads to a well defined localized level in the band gap whose occupancy leads to a change in the Ge-O bond length and hence to a change in vibrational mode. Here, we shall use this method to investigate the properties of the defect.

An important issue is the mechanism responsible for the annealing of VO and VO^- . Early Hall-effect measurements measured activation energies of about 0.9 eV in samples with *n*-type conductivity, independent of the dopant species.⁷⁻⁹ The small pre-exponential factor of about $\sim 10^7$ s^{-1} suggested a loss by migration.⁸ However, isothermal annealing experiments found VO anneals with an activation energy of 1.29 eV and a large pre-exponential factor (10^{12} – 10^{13} s^{-1}) indicating a dissociation process.⁹ Recently, DLTS measurements observed that the loss of VO^- was accompanied by a growth of the V-Bi complex, suggesting that

the dissociation is the predominant reaction responsible for the annealing. In order to clarify the picture, we perform a microscopic first-principles study of the migration and dissociation paths. The activation energies are calculated both for the neutral and negative charge states and are compared with the values reported in the literature. The understanding of the reactions that take place during this stage of annealing of oxygen-rich irradiated samples is essential in order to identify complexes that form at higher temperatures.

In the present paper, we investigate theoretically the properties of the A center, linking our findings with experiment whenever possible. Section II starts by describing the method used. There, we address an issue that, so far, has been ignored in the modeling of defects in germanium: the role of the semicore $3d$ orbitals of the Ge atoms. This problem is absent in the case of Si, a third row element, whose core is formed by the $1s^2 2s^2 2p^6$ deep electrons only. The results on the structure, electronic and vibrational properties, reorientation, diffusion, and dissociation are presented in Sec. III.

II. METHOD

A. General remarks

We use the local-density-functional cluster method AIM-PRO code.¹⁵ The core electrons were accounted for by using the dual space separable pseudopotentials of Hartwigsen *et al.*¹⁶

The basis set consists of Cartesian s -, p -, and d -type Gaussian functions centered on each atom. Ge atoms in the atom shells closer to the defect were treated with a basis consisting of (4, 4, 2) (s, p, d) Gaussian-type orbitals, whereas remote Ge atoms contribute with a contracted basis¹⁷ consisting of (4, 4, 1) (s, p, d) Gaussian orbitals optimized for bulk germanium. A basis of (4, 4, 4) (s, p, d) Gaussian orbitals with exponents optimized for the OGe_2H_6 molecule was placed at the oxygen site.

Octahedral, atom-centered clusters comprising a total number of 297 or 501 atoms were used in this study. The 297, 501, and 807 atom clusters are formed, respectively, by 181, 329, and 585 Ge atoms, whose surface dangling bonds were passivated with a total of 116, 172, and 222 H atoms. The positions of the germanium atoms were generated using the experimental lattice constant of Ge ($a_0 = 5.657 \text{ \AA}$).¹⁸ The defects were placed at the center of the clusters, which were then relaxed maintaining the outer Ge-H units locked in their initial positions. This relaxation at a fixed volume allows the comparison of the total energies of clusters containing different defect structures, and is essential to the calculation of electrical levels¹⁹ and diffusion barriers.

Vibrational modes were evaluated from the dynamical matrix related to the oxygen atom and its nearest Ge neighbors.¹² Test calculations show that an increase of only about 5 cm^{-1} in the O-related mode occurs when a larger shell of 16 Ge atoms is included in the dynamical matrix calculation.

Electric levels were calculated using the marker method.^{17,19,20} The position of the acceptor levels of the defect $E(q/q+1)$ relative to the valence or conduction band can

be found from the difference of the total energies of relaxed charged and neutral defects, $\Delta E_D(q/q+1) = E_D(q) - E_D(q+1)$. These are compared with analogous quantities found for a standard defect, designated *marker*, in the same sized cluster or supercell:

$$E(q/q+1)_D - E(q/q+1)_M = \Delta E_D(q/q+1) - \Delta E_M(q/q+1). \quad (1)$$

The marker has to be a defect with well established acceptor levels. It should also possess similar gap states so that its wave function and interaction with the cluster surface are as close as possible to those of the defect under scrutiny. We have chosen as a marker substitutional Au, which possesses well-known first and second acceptor levels at $E_v + 0.15 \text{ eV}$ and $E_c - 0.20 \text{ eV}$.²¹ These levels are close to the acceptor levels that we expect to obtain for VO. The atomic and electronic structures of substitutional Au are described in Ref. 22.

The diffusion and reorientation barriers were calculated by using the improved tangent nudged elastic band (NEB) method.²³ The starting point of the diffusion calculation are the initial and final structures, $\mathbf{R}_A \equiv \mathbf{R}_0$ and $\mathbf{R}_B \equiv \mathbf{R}_N$. The first chain of intermediate structures \mathbf{R}_i , with $i = 1, \dots, N-1$, named images, is generated by linear extrapolation of the initial and final structures. Each pair of successive images is coupled by a virtual elastic band, and the atoms of each image are moved until the forces vanish. The same method and number of images were successfully used before to calculate diffusion barriers in silicon.²⁴

B. Inclusion of nonlinear core corrected pseudopotentials

We now discuss the importance of the Ge $3d$ shell for an accurate description of the Ge-Ge and Ge-O bonds. The filled d shell has been shown to affect both the electronic and structural properties of many III-V and II-VI compounds, especially when bonds with first row elements are involved,²⁵ for example, in GaN, InN, GaP, GaAs, ZnS, and ZnO,²⁶⁻²⁹ and transition-metal impurities.

The energy levels of the free atoms provide an indication of the relevance of the core states (Fig. 1). GaN is a well-known example of non-negligible overlap (in this case between the $3d$ electron states of the Ga atom and the $2s$ orbitals of N) that in the free atoms differ by only $\sim 2 \text{ eV}$.²⁷ Ge occupies the adjacent position in the atomic table with the electronic configuration $[\text{Ar}]3d^{10}4s^2 4p^2$. As our goal is to model the interaction with the oxygen impurity atom, we are also concerned with the proximity of the O $2s$ levels to the Ge $3d$ levels and with the possible hybridization that can occur. Note that, obviously, this problem is absent in the case of Si.

This difficulty is avoided in all-electron calculations, where the problematic orbitals are treated explicitly, but the methodology is excessively time consuming and cannot be easily applied to large systems of atoms, as required to model defects in semiconductors. Louie *et al.*³⁰ introduced a scheme that accounts for the nonlinear nature of the exchange-correlation functional by explicitly adding a term dependent on the core charge density. This correction is

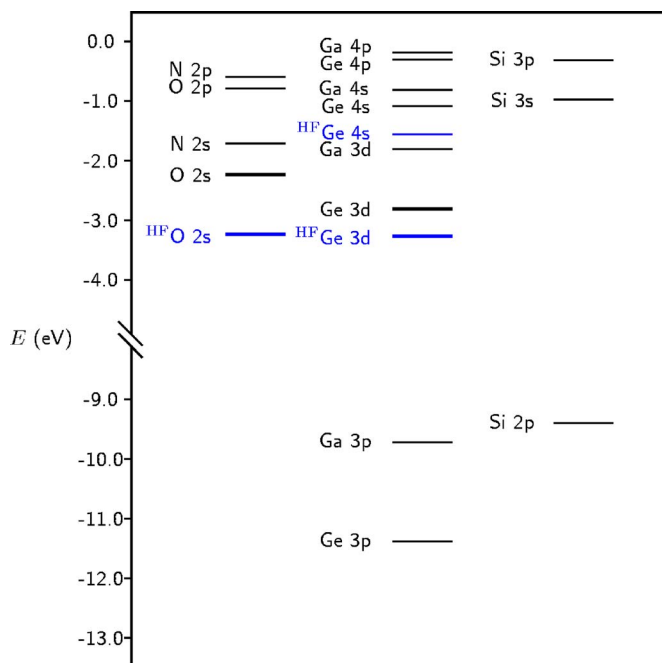


FIG. 1. (Color online) Atomic energy levels of the O, N, Ga, Ge, and Si elements. The density-functional-theory–local-density-approximation orbital energies are obtained from an all-electron relativistic calculation performed with the ADF code (Ref. 31). The Hartree-Fock (HF) values from Ref. 32 for the Ge 3d and 4s orbitals and the O 2s orbital are also shown for comparison. Despite the discrepancy between the absolute electron energies for the free atoms found in different references, the close proximity of the Ge 3d and O 2s orbitals suggests a significant hybridization.

known as the nonlinear core correction (NLCC).

Table I shows that the inclusion of NLCC makes little change in the calculated properties of bulk Ge. Our concern is whether it is important in the case of VO. Since the LVMs, which are measurable, reflect the Ge-O bond length, we use them as a test. We first perform structural optimizations of VO with and without NLCC, using the same starting point. The results are very different (Table II). With NLCC, the Ge-O bonds are 1.85 Å, and the normal frequency of vibration at 603 cm⁻¹ is very close to the measured 621 cm⁻¹.^{4,11} Neglecting the core orbitals, however, the O atom sinks from a bridging position toward near the substitutional site, result-

TABLE I. Calculated lattice parameter a_0 (Å), bulk modulus (GPa), and Raman frequency (cm⁻¹), with and without NLCC. The present results were obtained in two atom unitary cells of germanium. Experimental values are given for comparison.

	a_0 (Å)	B (GPa)	f_{Raman}
Without NLCC	5.584	73.2	299
NLCC	5.582	76.2	302
Expt.	5.657 ^a	76.5 ^b	300.7 ^c

^aAt 25 °C, from Ref. 18.

^bAt 77.4 K, Ref. 33.

^cReference 34.

TABLE II. Comparison of the calculated local vibrational modes (cm⁻¹) of the neutral VO defect and interstitial oxygen with and without NLCC. VO and O_i were modeled in clusters of 501 and 297 atoms, respectively. The experimental values are from Refs. 4, 11, 36, and 37.

Method	VO	O _i	
No NLCC	430	845	410
NLCC	603	863	416
Expt.	621	863	412

ing in the formation of long Ge-O bonds (2.03 Å).³⁵ The LVM drops to 430 cm⁻¹, well away from the experimental value. One may wonder why such different structures occur. The reason is that in all cases, the energy difference between the bridging site and the substitutional site is small. This is consistent with some experimental results on the reorientation energy of oxygen, which will be discussed later.

It is expected that Ge 3d orbitals also play a role in bonding with other defects in germanium. However, the effect is not so drastic if the energy surface for the atomic positions is not as flat as in the case of VO. In Table II, we include a similar test for interstitial oxygen. Although the Ge 3d orbitals also contribute in strengthening the Ge-O bonds there, the results are not as sensitive. In conclusion, the NLCC technique is required to model the properties of VO.

III. RESULTS

A. Structural details

In the stable VO defect with C_{2v} symmetry, shown in Fig. 2, the oxygen atom bridges two of the dangling bonds of the vacancy, while the other two form a reconstructed bond.

Details of the structure of the three charge states of VO are shown in Table III. The structural parameters are all within ~5% of the values previously reported for neutral VO.¹² In contrast, because the weakly reconstructed Ge-Ge

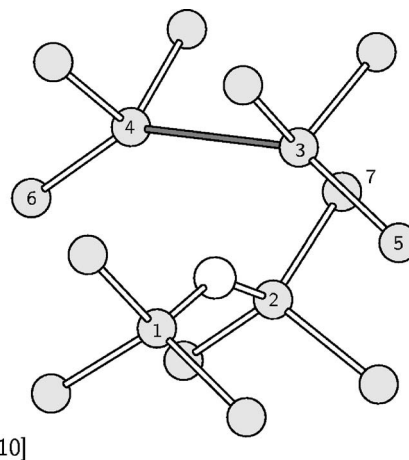


FIG. 2. The VO center. Germanium and oxygen atoms are represented in gray and white, respectively. The dark bond between atoms Ge₃ and Ge₄ represents a reconstructed bond.

TABLE III. Bond lengths (Å) and angles (deg) of the VO defect in germanium, shown in Fig. 2, calculated in a 501 atom cluster generated with the experimental lattice parameter. A “V” denotes the center of the vacancy and, in practice, is taken to be the center of the cluster.

	VO ⁰	VO ⁻	VO ⁼
O-Ge ₁	1.85	1.82	1.81
Ge ₁ -Ge ₂	3.48	3.54	3.54
O-V	0.97	1.24	1.25
Ge ₃ -Ge ₄	3.52	3.37	3.29
Ge ₁ -O-Ge ₂	140	154	156

bond introduces an antibonding level lying in the band gap of the cluster, we now find structural changes when electrons are added to the neutral defect. As it becomes more negative, the oxygen atom moves away from the vacancy center and the reconstructed bond shortens.

We carried out a test to check the convergence of the results with the cluster size by employing a 807 atom cluster to find the optimum structure of the neutral (single negative) VO. We obtained Ge-O bond lengths of 1.8347 (1.8176), 1.8502 (1.8164), and 1.8463 (1.8153) Å using 297, 501, and 807 atom clusters. The changes in the Ge-O bond length when the cluster is enlarged to 807 atoms are only 0.2% (0.06%). Of course, more computational effort is involved in the calculation of other properties such as local vibrational modes, and we had to use the smaller clusters of 297 or 501 atoms. However, this test supports the validity of the results.

B. Local vibrational modes

The normal modes of vibration of the VO center in the three charge states were calculated by finding the dynamical matrix of the central Ge₁-O-Ge₂ atoms. The asymmetric stretch of the oxygen atom, accompanied by an opposite movement of the Ge atoms, is located at 603 (621), 684 (669), and 694 (716) cm⁻¹ by our calculations

(experiment^{4,11}) for the neutral, negative and double negative charge states, respectively.

The calculated frequencies and respective isotope shifts are detailed in Table IV. The 669 and 716 cm⁻¹ bands show a fine structure due to the different isotope combinations arising from the five stable Ge isotopes ⁷⁰Ge, ⁷²Ge, ⁷³Ge, ⁷⁴Ge, and ⁷⁶Ge.^{4,11} Additionally, the band positions of the stretch mode in all the charge states have been measured in Ge doped with ¹⁸O. All the measured isotope shifts are in excellent agreement with our calculations.

When electrons are added to the defect, the oxygen atom moves away from the vacancy and the Ge-O bonds are shortened. We thus observe an upward shift of the frequency with the negative charge, as expected, but the calculated values of $f^- - f^0$ and $f^= - f^-$ are over estimated and underestimated, respectively.

C. Electronic levels and wave functions

Using substitutional Au as a marker, the two gap levels of VO are located at $E(-/0) = E_v + 0.30$ eV and $E(=/-) = E_c - 0.29$ eV, in excellent agreement with the measured activation energy for hole emission $E_h(-/0) = 0.32$ eV and enthalpy for electron emission $\Delta H_e(=/-) = 0.26$ eV, respectively.¹¹ The acceptor states calculated with the cluster, represented in Fig. 3, are very localized in the defect core.

In Si, the position of the acceptor level $E(-/0)$ was shown to be very dependent on the length of the reconstructed Si₃-Si₄ bond.³⁸ As the two dangling bonds reconstruct into a bond with length closer to the bulk Ge-Ge bonds, the gap level is expected to approach the conduction band.³ Using EPR, Watkins and Corbett characterized the wave function of the unpaired electron of VO⁻, showing that it was 70% localized in the Si₃ and Si₄ atoms and was nodal in the oxygen atom.³ Accordingly, first-principles calculations have shown that when the unpaired electron is added to the neutral VO defect, the Si₃-Si₄ bond distance increased as a consequence of the repulsion.³⁸

Figures 3(c) and 3(d) show the wave function of the VO⁻ paramagnetic state in Ge. The shape of the wave function is

TABLE IV. Local vibrational mode frequencies (cm⁻¹) for the VO center in germanium. Upper part of the table: Absolute frequencies of the B1 mode calculated for the ¹⁶O isotope in a ⁷⁴Ge host. Experimental frequencies are also given for comparison. The bracketed value is the position of the band in ^{nat}Ge since no isotope splitting was observed in this case. Lower part of the table: Isotope shifts of the B1 mode relative to the ^mO, ^MGe₁, and ^MGe₂ frequencies ($\delta f^{m,M,M}$). The average atomic weight of ^{nat}Ge was taken to be 72.64.

	Isotope masses O, Ge ₁ , Ge ₂	VO		VO ⁻		VO ⁼	
		Calc.	Expt.	Calc.	Expt.	Calc.	Expt.
$f^{16,74,74}$		603	[621.4] ^a	684	668.67 ^b	694	715.80 ^b
$\delta f^{16,74,74}$	16, 72, 72	0.7		0.8	0.83 ^b	0.8	0.92 ^b
	16, 74, 72	0.4		0.4	0.41 ^b	0.4	0.46 ^b
	18, 74, 74	-31.4		-35.9	-33.62 ^b	-36.3	
$\delta f^{16,nat,nat}$	18, nat, nat	-31.4	-31.8 ^a	-35.8	-33.7 ^a	-36.3	-35.8 ^a

^aReference 11.

^bReference 4.

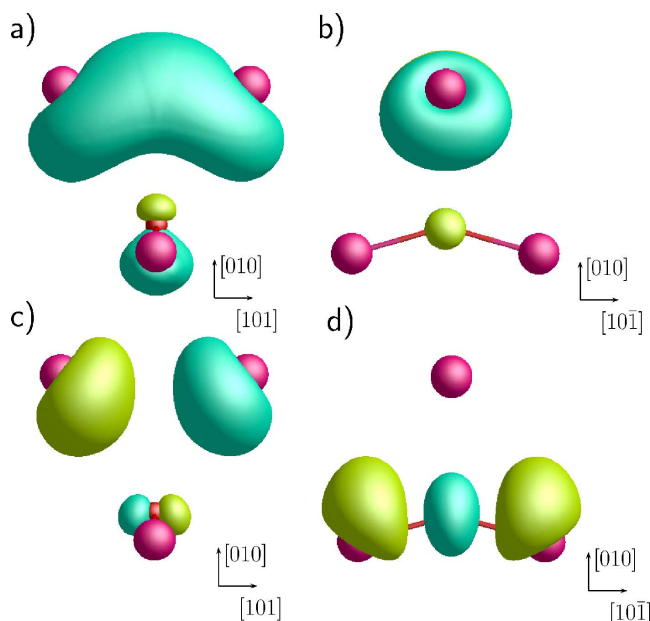


FIG. 3. (Color online) Representation of the electron wave function of the (a) highest occupied level of VO^0 , (b) and (c) highest occupied level of VO^- (two different projections), and (d) lowest unoccupied level of VO^- . The oxygen atom is represented as a small sphere and the germanium atoms are represented as large spheres.

similar to that deduced from the EPR experiments in Si, predominantly localized in the Ge_3 and Ge_4 atoms (43% of the charge density) and nodal in the mirror plane bisecting the bond formed by them and containing the O atom. Nevertheless, as shown in Table III, we found that the reconstructed bond was shorter in the negatively charged defect. Both in VO^0 and VO^- , the *total valence* charge density is located in the close neighborhood of the oxygen atom, although it is null on the oxygen atom itself. With the addition of the unpaired electron, the electronegative oxygen atom moves away from the vacancy center, thus diminishing the repulsion between the oxygen and the two dangling bonds.

D. Reorientation barrier

We investigated the reorientation barrier of oxygen within the vacancy cage using the NEB method in 501 atom clusters. This was accomplished by optimizing the positions of the O atom plus the 16 Ge atoms closer to the defect core in each image of the diffusion chain. The calculated barriers for reorientation are 0.11, 0.23, and 0.40 eV for VO^0 , VO^- , and VO^+ , respectively. The saddle point for the reorientation of VO is a C_{1h} structure represented in Fig. 4(b), where the oxygen is in the mirror plane between the initial and final configurations [Figs. 4(a) and 4(c)].

In Si, the corresponding reorientation barrier of VO^0 was found experimentally to be 0.38 eV,³ and as in germanium, the barrier increases as more electrons are added to the defect. The small activation energy required to change the position of the O atom inside the Ge vacancy and the increasing reorientation barrier with the number of added electrons are consistent with experiment. They explain the observation of

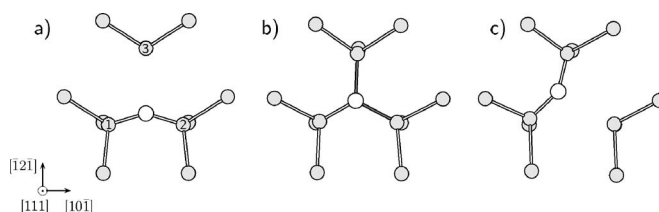


FIG. 4. Reorientation of VO^0 : (a) initial position, (b) saddle point, and (c) final position. Germanium and oxygen atoms are represented by gray and white spheres, respectively. In structure (b), two O-Ge bonds are represented in a darker shade to highlight that they are longer than the third Ge-O bond.

a stress-induced splitting of the ($=/-$) electron trap, where a uniaxial stress acting on a population of differently oriented VO^{\pm} defects shifts the level by an amount dependent on the orientation of the defect in the stress field. However, no such splitting was observed for the ($-/0$) emission peak (corresponding to a $\text{VO}^0 \rightarrow \text{VO}^- + h^+$ transition)¹¹ since at the temperature of the measurement, the defects could reorient and assume the lowest-energy orientation. The DLTS measurement was carried out at 140–200 K, implying that the initial neutral state is *thermally averaged* over all six equivalent C_{2v} lattice alignments. Therefore, its apparent T_d symmetry makes the observation of any level splitting impossible. Moreover, additional evidence for a low reorientation barrier for VO^0 comes from the fact that only the vibrational bands of VO^- and VO^+ show a fine structure due to different Ge isotopic configurations even at 15 K.^{11,4}

E. Diffusion and dissociation

We now investigate the migration barrier of VO as a unit and its barrier to dissociation into a free vacancy and an oxygen interstitial. These activation energies are found using the climbing NEB method.

As previously described, five images which are snapshots lying on the trajectory between the initial and final positions are selected by linear interpolation and are subsequently relaxed subject to spring forces from neighboring images.³⁹ During the image relaxations, the positions of O and all Ge atoms not attached to H terminators were optimized. As a test, we employed a similar method to calculate the activation energy for the hopping of an interstitial oxygen atom obtaining 2.35 eV, in very good agreement with the experimental value of 2.08 eV.⁴⁰

To guarantee that the true saddle point was found, we repeated the calculation to check the presence of more than one energy barrier in the transformation, introducing five images between each energy minimum and calculating separately each saddle point. These calculated energy barriers represent an improvement over those reported previously.⁴¹

Several possible dissociation and migration paths were investigated. We found that in all the cases, the minimum energy paths could be decomposed into single transformations between VO and a metastable vacancy-oxygen pair, which we designate as VO^* , where O lies close to a bond center site near V. This defect, shown in Fig. 5(c), is 0.52 (0.40) eV higher in energy than VO in the neutral (single

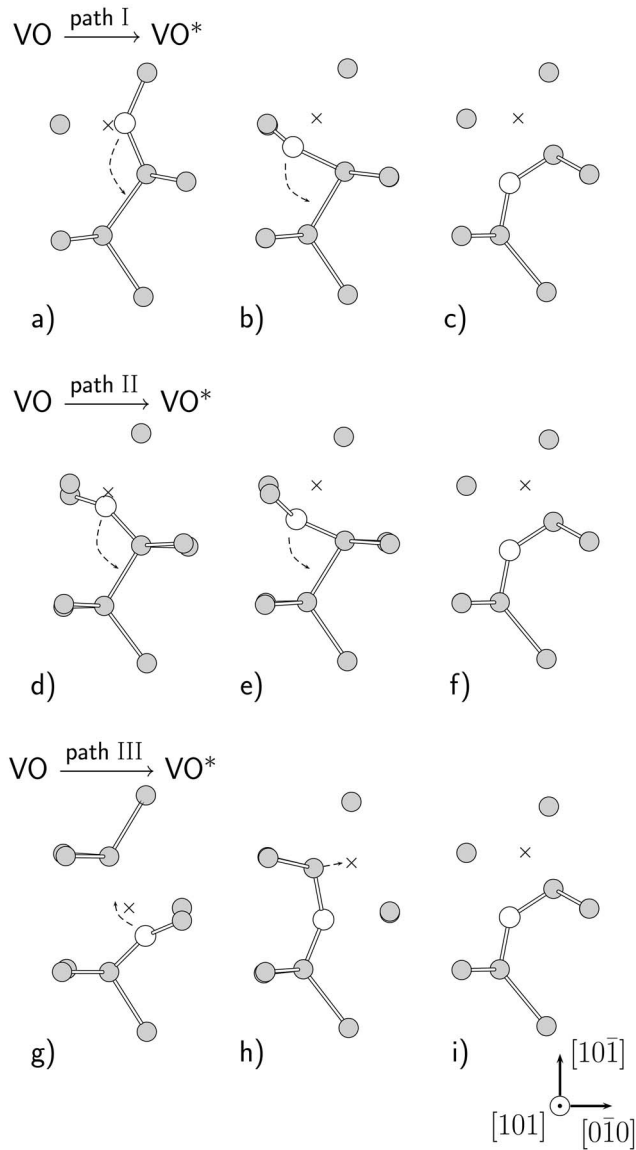


FIG. 5. Diffusion paths: [(a)–(c)], [(d)–(f)], and [(g)–(i)] are three possible mechanisms of transformation of VO into a metastable structure VO*. Germanium and oxygen atoms are represented by gray and white spheres, respectively. Crosses indicating the vacancy site and dashed arrows suggesting the movement of the atoms were added to help in the visualization.

negative) charge state. A metastable configuration obtained by exchanging the positions of the vacancy and one of the atoms Ge₃ or Ge₄, was ruled out since it was found to relax spontaneously to VO.

Three possible paths for the transformation VO → VO* are depicted in Figs. 5(a)–5(c) (labeled path I), 5(d)–5(f) (path II), and 5(g)–5(i) (path III). The relative orientations of the initial VO defect and the final VO* structure are different in each case. Path A consists in a jump of the oxygen atom into a neighboring Ge-Ge bond in the same plane as the initial Ge₁-O-Ge₂ triangle. Even though the symmetry was not restricted during the NEB calculation, the oxygen atom moved nearly without leaving the [101] mirror plane. Path II is also a jump of the oxygen atom, but occurs out of the

TABLE V. Activation energies (eV) for the transformations VO → VO* and VO* → V+O depicted in Fig. 5 and the resulting minimum migration and dissociation barriers (E_{mig} and E_{diss}). All the values were calculated using 297 atom clusters. Experimental values are from Refs. 7–9 and 44.

Reaction	VO ⁰	VO ⁻
path I VO → VO*	1.2	1.1
path II VO → VO*	1.1	0.9
path III VO → VO*	1.2	0.9
VO* → V+O	1.0	0.7
Migration	1.2	0.9
Dissociation	1.5	1.1
Expt. (migration)		0.90–0.94
Expt. (dissociation)	~1.29	~1.25

plane. In path III, the oxygen carries out a reorientation, and thereafter keeps its two Ge-O bonds while the vacancy jumps to a neighboring site. All the transformations have nearly the same activation energies. These are listed in Table V. A succession of transformations VO $\xrightarrow{\text{path I or II}}$ VO* $\xrightarrow{\text{path III}}$ VO or the reciprocal process VO $\xrightarrow{\text{path III}}$ VO* $\xrightarrow{\text{path I or II}}$ VO composes a migration step. The dominant energy barrier for the lowest-energy migration process (E_{mig}) is given in Table V, and the respective energy profile is represented in Fig. 6.

VO* can also be an intermediate step in the dissociation. Figures 7(a)–7(c) shows V jumping to a position farther away from O. The dissociated pair V+O in Fig. 7(c) is 0.62 (0.55) eV higher in energy than neutral (single negative) VO*. We tested different alternative reconstructions of the

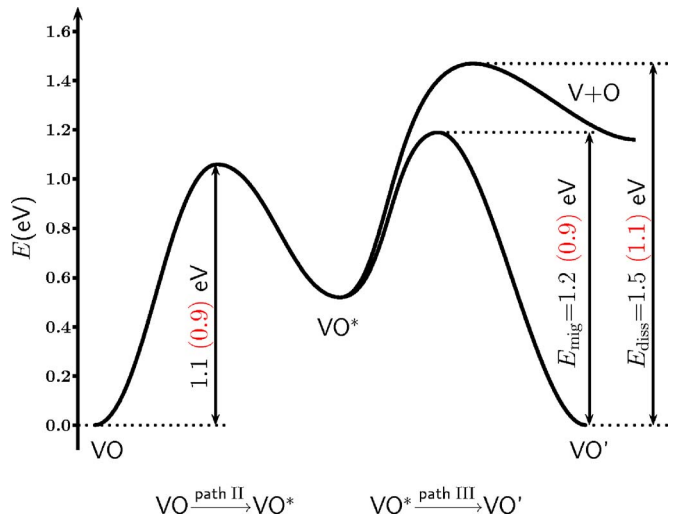


FIG. 6. (Color online) Proposed configuration-coordinate diagram for the VO defect including the relevant transformations involved in the lowest-energy migration and dissociation mechanisms. VO and VO' represent equivalent vacancy-oxygen defects centered in different lattice sites. The corresponding energies for the single negatively charged defect are given in parentheses.

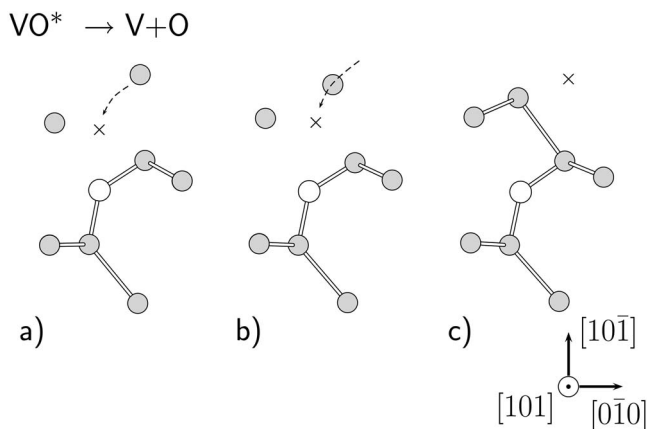


FIG. 7. Second step of the dissociation path of VO from (a) VO^* to (c) $V+O$. Crosses indicate the vacancy site.

vacancy neighboring the oxygen site to find the lowest-energy $V+O$ structure, and thus the relative energy is slightly lower than those found in our previous work.⁴¹ The respective activation energy E_{diss} , obtained by adding $E(VO^*) - E(VO)$ to the energy barrier of the second step $VO^* \rightarrow V+O$, is given in Table V.

The calculated energy barriers show that the activation energy for dissociation is larger than the activation energy for migration in both the neutral and single negative charge states. Nevertheless, this does not mean that migration rates will always be larger than dissociation rates as the pre-exponential factors are different.^{8,9} The rate at which the migrating VO species encounters and reacts with other defects or impurities such as interstitial oxygen or vacancies depends on the concentration of traps.

Hall-effect, IR spectroscopy, and DLTS measurements show the annealing of VO^0 , VO^- , and $VO^=$ at around 150 °C.^{8,9,13,42} Our activation energies of 1.2 and 0.9 eV for the migration of VO and O^- , respectively, suggest an approximate annealing temperature of $W/(k \ln \nu)$, where $\nu \sim 10^{13} \text{ s}^{-1}$ is an atomic jump frequency. This simple model yields temperatures of about 192 and 80 °C, respectively, entirely consistent with experiment.

The calculated energy barriers can be compared directly with the measured activation energies for annealing if a single (or dominant) loss mechanism is assumed. Differences were observed depending on the characteristics of the samples used. In Bi-doped samples, the annealing of VO at about 150 °C was followed by a growth of the concentration of the bismuth-vacancy (BiV) pair, suggesting that the vacancies released by the dissociation of VO are trapped by the Bi impurity.⁴³ Fitting the DLTS data, a barrier of about $W \sim 1.25 \text{ eV}$ is estimated,⁴⁴ which compares very well with the 1.1 eV required for the dissociation of VO^- . In contrast, in Ge doped only with oxygen and submitted to similar irradiation and annealing conditions, IR measurements have reported the formation of several groups of oxygen-related defects. Some of these were assigned to VO_2 defects,^{8,9,13} indicating that VO migrates as a unit, without dissociating, and forms VO_2 when trapped by interstitial oxygen. Electrical measurements on Sb-, As- and P-doped samples, on the other hand, suggested that VO^- anneals by migration with an

activation energy of 0.90–0.94 eV,^{7,8} while in Ga-doped material a pre-exponential factor several orders of magnitude higher suggests a loss by dissociation, with an activation energy of 1.29 eV.⁹ Both agree with our calculated activation migration barrier of VO^- and dissociation barrier of VO^0 (0.9 and 1.5 eV, respectively). In the Ga-doped samples, it is likely that the defects were partially in the negative charge state, justifying why the measured activation energy is smaller. The observation of different qualitative behaviors in different studies is linked well with the case of Si, where experimental annealing curves were well described by a model incorporating both a migration-constrained reaction and dissociation, with comparable activation energies.⁴⁵

IV. CONCLUSIONS

We have carried out density-functional calculations of the properties of the VO center in Ge using large H-terminated clusters. It was shown that it is important to include the Ge 3d shell in a description of the Ge-O bonds in the VO center. This can be achieved by using a NLCC correction. It suggests that this kind of interaction may be required for modeling other oxygen-related defects in germanium.

The theory confirms the C_{2v} symmetry of the center and determines the position of its two acceptor levels at $E(-/0) = E_v + 0.30 \text{ eV}$ and $E(=/-) = E_v - 0.29 \text{ eV}$, which are within 0.03 eV of the experimental values. We also qualitatively reproduce the upward frequency shift of the O-related local vibrational mode with charge state.

The reorientation barriers of VO^0 , VO^- , and $VO^=$ were found to be 0.11, 0.23, and 0.40 eV, respectively. The ease of reorientation of VO^0 , even at low temperatures, explains the absence of Ge isotopic fine structure of the 621 cm^{-1} band,^{4,11} and the higher reorientation barriers of the charged states account for a stress-induced splitting of the $(=/-)$ level detected in Laplace DLTS studies.¹¹

The diffusion and dissociation mechanisms of VO involve a metastable form, VO^* , as an intermediate step in both processes. The calculated energy barriers for migration and dissociation are 1.2 (0.9) and 1.5 (1.1) eV for VO^0 (VO^-). Although the dissociation barrier is lower than the migration barrier, the pre-exponential factor for loss by migration to a sink is typically lower than that for loss by dissociation. These energies are consistent with experimental annealing temperatures around 150 °C and the activation energies reported for both *p*- and *n*-doped samples.⁷⁻⁹ As in Si, both dissociation and migration followed by trapping by other defects, are responsive for the annealing of the A center.⁴⁵ The dominating mechanism will depend on the sample characteristics such as Fermi level and concentration of traps.

ACKNOWLEDGMENTS

The authors are grateful to V. Markevich and C. Janke for valuable suggestions and comments. The Portuguese foundation Fundação para a Ciência e para a Tecnologia and the INTAS-03-50-4529 program are acknowledged for financial support.

*Electronic address: carvalho@excc.ex.ac.uk

- ¹J. A. Baldwin, *J. Appl. Phys.* **36**, 793 (1965).
- ²R. E. Whan, *Phys. Rev.* **140**, A690 (1965); *Appl. Phys. Lett.* **6**, 221 (1965).
- ³G. D. Watkins and J. W. Corbett, *Phys. Rev.* **121**, 1001 (1961); **121**, 1015 (1961).
- ⁴P. Vanmeerbeek, P. Clauws, H. Vrielinck, B. Pajot, L. Van Hoo-rebeke, and A. Nylandsted Larsen, *Phys. Rev. B* **70**, 035203 (2004).
- ⁵V. Nagesh and J. W. Farmer, *J. Appl. Phys.* **63**, 1549 (1988).
- ⁶J. Fage-Pedersen, A. N. Larsen, and A. Mesli, *Phys. Rev. B* **62**, 10116 (2000).
- ⁷N. Fukuoka and H. Saito, *Jpn. J. Appl. Phys.* **13**, 1524 (1974).
- ⁸V. V. Litvinov, V. I. Urenev, and V. A. Shershel, *Fiz. Tekh. Polu-provodn. (S.-Peterburg)* **17**, 1632 (1983).
- ⁹V. V. Litvinov, V. I. Urenev, and V. A. Shershel, *Fiz. Tekh. Polu-provodn. (S.-Peterburg)* **18**, 707 (1984).
- ¹⁰V. P. Markevich, I. D. Hawkins, A. R. Peaker, V. V. Litvinov, L. I. Murin, L. Dobaczewski, and J. L. Lindström, *Appl. Phys. Lett.* **81**, 1821 (2002).
- ¹¹V. P. Markevich, V. V. Litvinov, L. Dobaczewski, J. L. Lindström, L. I. Murin, S. V. Vetrov, I. D. Hawkins, and A. R. Peaker, *Physica B* **340-342**, 844 (2003).
- ¹²J. Coutinho, R. Jones, P. R. Briddon, and S. Öberg, *Phys. Rev. B* **62**, 10824 (2000).
- ¹³P. Vanmeerbeek and P. Clauws, *Phys. Rev. B* **64**, 245201 (2001).
- ¹⁴A. Seidl, A. Görling, P. Vogl, J. A. Majewski, and M. Levy, *Phys. Rev. B* **53**, 3764 (1996).
- ¹⁵P. R. Briddon and R. Jones, *Phys. Status Solidi B* **217**, 131 (2000).
- ¹⁶C. Hartwigsen, S. Goedecker, and J. Hutter, *Phys. Rev. B* **58**, 3641 (1998).
- ¹⁷J. Coutinho, V. J. B. Torres, R. Jones, A. Carvalho, S. Öberg, and P. R. Briddon, *Phys. Rev. B* **73**, 235213 (2006).
- ¹⁸*CRC Handbook of Chemistry and Physics*, edited by D. R. Lide, 81st ed. (CRC, Boca Raton, FL, 2000).
- ¹⁹A. Resende, R. Jones, S. Öberg, and P. R. Briddon, *Phys. Rev. Lett.* **82**, 2111 (1999).
- ²⁰J. Coutinho, V. J. B. Torres, R. Jones, and P. R. Briddon, *Phys. Rev. B* **67**, 035205 (2003).
- ²¹V. V. Ostroborodova, *Sov. Phys. Solid State* **7**, 484 (1965).
- ²²J. Coutinho, R. Jones, V. J. B. Torres, M. Barroso, S. Öberg, and P. R. Briddon, *J. Phys.: Condens. Matter* **17**, L521 (2005).
- ²³G. Henkelman and H. Jónsson, *J. Chem. Phys.* **113**, 9978 (2000).
- ²⁴N. Fujita, R. Jones, J. P. Goss, P. R. Briddon, T. Frauenheim, and S. Öberg, *Appl. Phys. Lett.* **87**, 021902 (2005).
- ²⁵D. Porezag, M. R. Pederson, and A. Y. Liu, *Phys. Rev. B* **60**, 14132 (1999).
- ²⁶K. Karch, F. Bechstedt, and T. Pletl, *Phys. Rev. B* **56**, 3560 (1997).
- ²⁷Vicenzo Fiorentini, Michael Methfessel, and Matthias Scheffler, *Phys. Rev. B* **47**, 13353 (1993).
- ²⁸A. F. Wright and J. S. Nelson, *Phys. Rev. B* **50**, 2159 (1994).
- ²⁹S.-H. Wei and Alex Zunger, *Phys. Rev. B* **37**, 8958 (1988).
- ³⁰S. G. Louie, S. Froyen, and M. L. Cohen, *Phys. Rev. B* **26**, 1738 (1982).
- ³¹G. te Velde, F. M. Bickelhaupt, S. J. A. van Gisbergen, C. Fonseca Guerra, E. J. Baerends, J. G. Snijders, T. Ziegler, *J. Comput. Chem.* **22**, 931 (2001); C. Fonseca Guerra, J. G. Snijders, G. te Velde, and E. J. Baerends, *Theor. Chem. Acc.* **99**, 391 (1998); ADF2005.01, SCM, Theoretical Chemistry, Vrije Universiteit, Amsterdam, The Netherlands, <http://www.scm.com>
- ³²J. C. Slater, *Phys. Rev.* **98**, 1039 (1955).
- ³³H. J. McSkimin and P. Andreatch, Jr., *J. Appl. Phys.* **34**, 651 (1963).
- ³⁴J. H. Parker, Jr., D. W. Feldman, and M. Ashkin, *Phys. Rev.* **155**, 712 (1967).
- ³⁵The reason why the previous calculations by some of us (Ref. 12) did not show this problem is not clear to us. This may be related to the fact that a smaller set of real-space basis functions was used, and some of them were placed in the bond centers. Also, it may have resulted from strain in the smaller 64 atom supercell used.
- ³⁶E. Artacho, F. Ynduráin, B. Pajot, R. Ramírez, C. P. Herrero, L. I. Khirunen, K. M. Itoh, and E. E. Haller, *Phys. Rev. B* **56**, 3820 (1997).
- ³⁷A. J. Mayur, M. D. Sciacca, M. K. Udo, A. K. Ramdas, K. Itoh, J. Wolk, and E. E. Haller, *Phys. Rev. B* **49**, 16293 (1994).
- ³⁸A. Resende, Ph.D. thesis, University of Exeter, 1999.
- ³⁹G. Henkelman, B. P. Uberuaga, and H. Jónsson, *J. Chem. Phys.* **113**, 9901 (2000).
- ⁴⁰J. W. Corbett, and G. D. Watkins, *J. Phys. Chem. Solids* **25**, 873 (1964).
- ⁴¹A. Carvalho, R. Jones, J. Coutinho, M. Shaw, V. J. B. Torres, S. Öberg, and P. R. Briddon, *Mater. Sci. Semicond. Process.* **9**, 489 (2006).
- ⁴²V. P. Markevich, V. V. Litvinov, L. Dobaczewski, J. L. Lindström, L. I. Murin, and A. R. Peaker, *Phys. Status Solidi C* **0**, 702 (2003).
- ⁴³V. P. Markevich, A. R. Peaker, V. V. Emtsev, V. V. Litvinov, and L. I. Murin, *Physica B* **376-377**, 93 (2006).
- ⁴⁴V. P. Markevich (private communication).
- ⁴⁵B. G. Svensson and J. L. Lindström, *Phys. Rev. B* **34**, 8709 (1986).